ELSEVIER

Journal of Alloys and Compounds 469 (2009) 66–72

Journal of ALLOYS AND COMPOUNDS

www.elsevier.com/locate/jallcom

Thermal and electrothermal characterization of bismuth based high-T_c superconductors

M. Anis-ur-Rehman *

Applied Thermal Physics Laboratory, Department of Physics, COMSATS Institute of Information Technology, Islamabad, Pakistan

Received 19 December 2007; received in revised form 1 February 2008; accepted 7 February 2008
Available online 14 February 2008

Abstract

This paper investigates the relationships among macroscopic physical properties and features at atomic level for the high-T_c superconducting material with nominal composition $Bi_{1.6}Pb_{0.4}Sr_{1.6}Ba_{0.4}Ca_2Cu_3O_y$, which was prepared by a solid-state reaction method. The samples were analyzed by dc electrical resistivity, ac susceptibility, thermal transport, electrothermal conductivity and thermoelectric properties all as a function of temperature (from room down to LN_2 temperature). Room temperature X-ray diffraction studies were also done. All the above measurements showed that in the samples, there exists almost a single high-T_c phase with $T_{c,0} \simeq 110 \pm 1$ K. The lattice constants of the material were determined by indexing the diffraction peaks. Samples are investigated for thermal transport properties, i.e. thermal conductivity, thermal diffusivity and heat capacity per unit volume, by an advantageous transient plane source method. Simultaneous measurement of thermal conductivity and thermal diffusivity makes it possible to estimate specific heat and the Debye temperature Θ_D. Thermoelectric power (Seebeck coefficient) and electrothermal conductivity is also measured with a newly developed and calibrated apparatus. Using electrical resistivity, thermal conductivity and thermoelectric power, the Figure of merit factor was calculated.

Keywords: High-T_c superconductors; Thermoelectric materials; Solid-state reactions; Crystal structure; Electron–phonon interactions; Heat capacity; Heat conduction; Phase transitions; Thermoelectric; Thermal analysis; X-ray diffraction

1. Introduction

Dissipation phenomena in high temperature superconductors are governed by the microstructure that develops during the preparation process. Therefore, detailed investigations of the electrical and thermal transport and ac magnetic susceptibilities in superconductors prepared either in the form of single crystals, thin films or polycrystalline are important for understanding superconductivity as well as for practical applications.

The effect of elements (Pb, Fe, Co, Ni, Zn) doping in Bi-based superconducting materials have been extensively investigated [1–8]. It was reported that the superconducting properties of these materials decrease with increase of the amount of doping, regardless of the nature of the dopants. The suppression of superconductivity was concluded to be due to local disorder induced by the amount of doping. However, the details of the current limiting mechanisms in the Bi-2223 system are not well established. Consequently, it is of interest to try these doping elements in the Bi-2223 system with a different nominal composition, of which we intend to investigate $Bi_{1.6}Pb_{0.4}Sr_{1.6}Ba_{0.4}Ca_2Cu_3O_y$ in order to provide additional observations to contribute further understanding of their role on the superconductivity of the system.

It is well established that ceramic high-T_c superconductors comprise a collection of tiny, randomly oriented anisotropic grains which are connected to each other by a system of so called 'weak links' or 'matrix'. The linear temperature dependence of the electrical resistivity is one of the most important properties of the normal phase kinetics of high-T_c layered cuprates [9].

In superconductors where the dc electrical resistivity diverges to zero below T_c, the thermal conduction is almost a unique measurement to study the transport properties below T_c. The magnitude and temperature dependence of the thermal conductivity are parameters which have an impact on a broad spectrum of devices. In high-T_c superconductors, such information is even more valuable to know how the free carriers and lattice vibrations contribute to the transport of heat. Transient Plane Source (TPS) technique is a well developed and a well known method [10–12] to study the thermal transport properties. For TPS method single

* Tel.: +92 321 5163059.
E-mail addresses: marehman@comsats.edu.pk, rehmananis@hotmail.com.

0925-8388/$ – see front matter © 2008 Elsevier B.V. All rights reserved.
doi:10.1016/j.jallcom.2008.02.023

transition phase will be of great help to study such properties. Multiple phases, in the material, will make the situation more complicated and increase in measurement errors also. The TPS technique is modified and improved for the measurements of thermal transport properties of high-T_c superconductors. The modified arrangement is referred to as the advantageous transient plane source (ATPS) technique [13].

The circuit components are reduced with this new arrangement as compared to the bridge used earlier [14]. The modified bridge arrangement is already calibrated with fused quartz, carbon steel and AgCl crystals [13,15].

Peltier refrigerators use the thermoelectric materials for refrigeration. Peltier thermoelectrics are more reliable than compressor based refrigerators, and are used in situations where reliability is critical like deep space probes. Thermoelectric material applications include refrigeration or electrical power generation. Thermoelectric materials used in the present refrigeration or power generation devices are heavily doped semiconductors. The metals are poor thermoelectric materials with low Seebeck coefficient and large electronic contribution to the thermal conductivity. Insulators have a large Seebeck coefficient and a small contribution to the thermal conductivity, but have too few carriers, which result in a large electrical resistivity. The Figure of merit is the deciding factor for the quality of thermoelectric materials. In order to increase the whole Figure of merit, it is of interest to replace the p-type leg of the Peltier junction by a thermoelectrically passive material with a Figure of merit close to zero [16]. This is why it is interesting to study the Figure of merit of the ceramic superconductors.

One of the important thermomagnetic transport quantities is the electrothermal conductivity and is shown to be one of the powerful probes of high-temperature superconductors. Cryogenic bolometers are sensitive detectors of infrared and millimeter wave radiation and are widely used in laboratory experiments as well as ground-based, airborne, and space-based astronomical observations [17]. In many applications, bolometer performance is limited by a trade off between speed and sensitivity. Superconducting transition-edge bolometer can give a large increase in speed and a significant increase in sensitivity over technologies now in use. This combination of speed with sensitivity should open new applications for superconducting bolometric detectors [18].

Other potent applications for electrothermal conductivity of superconductors is actuators in MEMS technologies, electrothermal rockets, etc. [19].

The temperature dependence of the dc electrical resistivity, along with low field ac magnetic susceptibility, X-ray diffraction, thermal transport, electrothermal conductivity and thermoelectric power studies and calculations of Figure of merit factor are undertaken in this paper.

2. Experimental

2.1. Preparation and characterization

In the Bi-based high-T_c superconductors the Bi-2223 phase is stable within a narrow temperature range and exhibits phase equilibria with only a few of the compounds existing in the system [20]. Precise control over the processing parameters is required to obtain the phase-pure material [21].

All specimens were prepared from 99.9% pure powders of Bi_2O_3, PbO, $SrCO_3$, $BaCO_3$, $CaCO_3$ and CuO. The powders were mixed to give nominal composition of $Bi_{1.6}Pb_{0.4}Sr_{1.6}Ba_{0.4}Ca_2Cu_3O_y$ and were thoroughly ground in an agate mortar to give very fine powder. The grind powder was calcined for 21 h in air at 800 °C. A series of pellets was produced in two sizes, from this well mixed material and controlled heating and cooling carried out, in air, using a horizontal tube furnace. Poly vinyl alcohol (PVA) was used as binder in the samples. PVA is one of the few high molecular weight commercial polymers, which is water soluble and is dry solid, commercially available in granular or powder form. The properties of poly vinyl alcohol vary according to the molecular weight of the parent poly vinyl acetate and the degree of hydrolysis. Fully hydrolysed form with medium viscosity grade PVA was used in our case. Samples were in the shape of cylindrical disks having diameters 13 and 28 mm, and lengths 3 and 11 mm, respectively. These samples were sintered at 830 °C for the intervals of 24 h in each sintering step as sintering procedures do affect the properties [22].

The superconducting properties were characterized electrically by using standard four-probe method. Contacts were made by high quality silver paste. The temperature was measured by using a calibrated Pt-100 thermometer.

Low field ac susceptibility measurements are very important for the characterization of high-temperature superconductors [23–26]. The sharp decrease in the real part $\chi'(T)$ below the critical temperature T_c is a manifestation of diamagnetic shielding. ac susceptibility of the sample was measured after each sintering step. The low field ac susceptibility properties were studied by the use of mutual inductance bridge method. The measurements were taken from room temperature down to 80 K.

X-ray diffractograph (XRD) of sample was taken after the final sintering. The radiation used for XRD was Cu Kα and the measurements were made at room temperature. Measurements were done at room temperature since there is no change in the structure of the superconducting materials before and after transition [22,27].

2.2. Thermal transport properties

Thermal transport measurements, i.e. thermal conductivity, thermal diffusivity and heat capacity per unit volume were performed using the advantageous transient plane source (ATPS) technique [13,15]. Circuit diagram for the method is shown in Fig. 1. Simultaneous measurement of thermal conductivity and thermal diffusivity is the foremost advantage of this technique. Heat capacity per unit volume is then calculated using the idea that, if all heat is transported via solid specimen then the thermal conductivity (λ), thermal diffusivity (κ) and heat capacity per unit volume (ρC_p) are expressed by

$$\kappa = \frac{\lambda}{\rho C_p} \quad (1)$$

A detailed description of this experimental technique can be found elsewhere [10]. The ideal model presupposes that the double spiral sensor, assumed to consist of a set of equally spaced, concentric, and circular line heat sources, is sandwiched in specimens of infinite dimensions. In practice all real specimens do have finite dimensions. However, by restricting the time of the transient, which relates to the thermal penetration depth of the transient heating, a measurement can still be analyzed as if it was performed in an infinite medium. This means that the ideal theoretical model is still valid within a properly selected time window for the evaluation. The scatter in thermal conductivity measurements is about 0.14% and is 0.66% and 0.52% in thermal diffusivity and volumetric heat capacity respectively [13,15]. Taking into consideration the limitations of the theory of the technique and the experimental sampling errors, the thermal conductivity and thermal diffusivity data contain errors of 4% and 7%, respectively. The errors in volumetric heat capacity are around 10% [13–15].

2.3. Thermoelectric power measurements

An easy to use and simple apparatus was designed and developed for thermoelectric power (S) measurements. Circuit diagram along with the sample holder assembly is shown in Fig. 2.

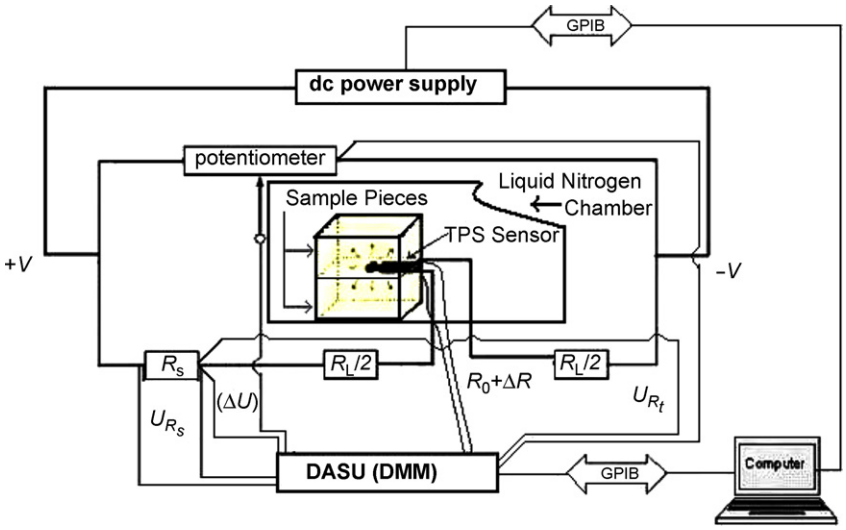

Fig. 1. Circuit diagram for the advantageous transient plane source (ATPS) technique.

The sample is subjected to a temperature difference ΔT by using a heating resistor and corresponding voltage difference ΔV across the sample is measured. Thermoelectric power is obtained by taking ratio of the voltage difference to the temperature difference. Chromel–alumel thermocouples are used for measuring the temperature difference, ΔT. The thermocouples are electrically isolated from the sample and thermally connected to the sample. Heat losses through the electrical connections are minimized by using long leads wrapped around a Teflon tube. The voltage leads are then silver pasted to the sample in the vicinity of thermocouples to assure that the voltage and temperature gradients are measured at the same locations on the sample for accurate thermoelectric power measurements. The next step includes loading the sample assembly into the sample chamber and evacuation of the chamber. The chamber is evacuated to eliminate any water vapour condensation on the sample, which can result in erroneous measurements. Dry nitrogen gas is then filled in the chamber as a conducting media between chamber walls and the sample. This sample chamber is then inserted in liquid nitrogen container for cooling. Data are collected under the computer control. By incorporating multiple measurements in a single run, considerable time is saved by avoiding remounting, and recooling of the samples. In this technique the surface mount resistor (50 Ω) was used to heat one end of the sample to establish a measured temperature gradient of approximately 1 K.

3. Experimental results and discussion

3.1. dc electrical resistivity

Variation of resistivity with change in temperature is recorded for after each sintering step and the plots are given in Fig. 3. One of the most striking features about the cuprate superconductors is the behavior of the resistivity of the normal state that is found above the transition temperature of the optimally doped materials. After the final sintering the measured density of the sample was 3.48 g cm^{-3} and $T_{c,0}$ was 110 ± 1 K. The added barium (Ba) has increased the $T_{c,0}$. Residual resistivity was 0.19 mΩ cm and the intrinsic resistivity was 5.9 μΩ cm K^{-1}. The ratio $\rho(273\,\text{K})/\rho(4.2\,\text{K})$ is the residual resistivity ratio (RRR), an important parameter in the design of superconductive applications. In the case of a superconductor, the denominator has to be taken at a temperature slightly above the critical temperature [28]. RRR in our case was in the range 23–33.

3.2. ac susceptibility

ac susceptibility measurements were done after each sintering step (Fig. 4). Initially two transition phases were present. One of the identified phases is the Bi-2212(low-T_c) phase and the other Bi-2223(high-T_c) phase. With sintering,

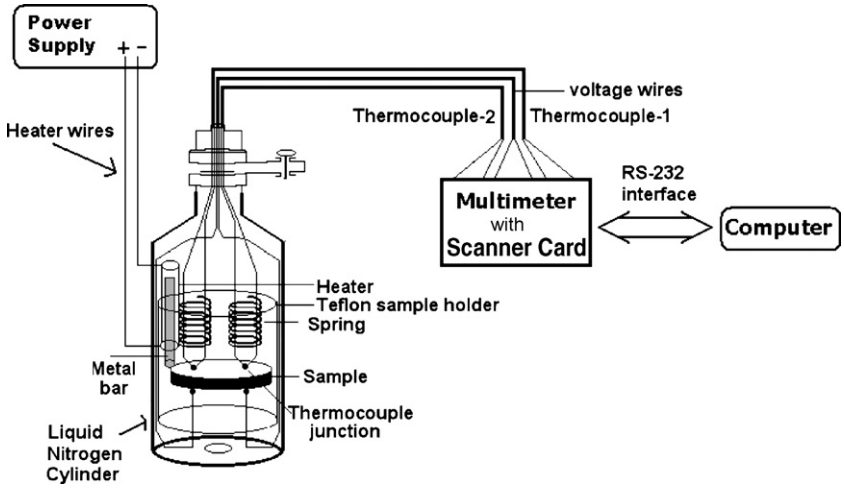

Fig. 2. Block diagram of the apparatus developed for thermoelectric power measurements. Scanner card is used with the multimeter for simultaneous measurements at different points as shown. RS-232 is the standard serial interface of the computer.

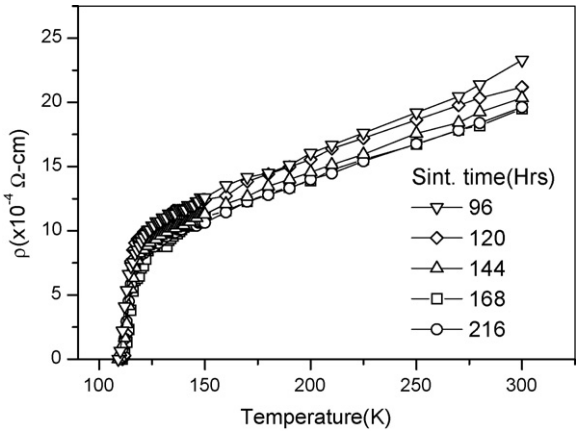

Fig. 3. dc electrical resistivity as a function of temperature for the sample after each sintering step.

the low-T_c phase was smoothed out and only phase left is the Bi-2223(high-T_c) phase. Although the resistivity variation with temperature was smoothed out after the third sintering but slight kinks were observed in the susceptibility against temperature plot showing the more sensitivity of the measuring method.

3.3. X-ray diffraction studies

Almost all the peaks are indexed. The only phase is the orthorhombic high-T_c Bi-2223 phase. Lattice parameters were calculated from the ($h\,k\,l$) values of the indexed peaks. The lattice parameters are $a = 5.42$ (1) Å, $b = 5.37$ (1) Å and $c = 37.12$ (8) Å. No peaks were found matching the Bi-2212 low-T_c phase. Indexed X-ray diffractograph is shown in Fig. 5. The lattice constants agreed with the previous reports [12]. The size of the grains in polycrystalline materials has pronounced effects on many of its properties. Using Scherrer's equation [29]:

$$B = \frac{0.9\lambda}{t\cos\theta}, \tag{2}$$

where B is the broadening of diffraction line measured at half its maximum intensity (radians), λ the radiation source wavelength and t is the diameter of crystal particle, particle sizes are determined and the diameter of the crystal particles lies between 172 and 512 Å.

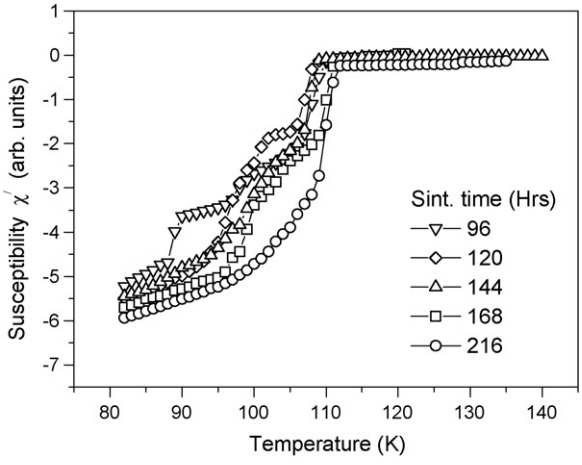

Fig. 4. Variation of ac susceptibility (real part), with temperature after each sintering step.

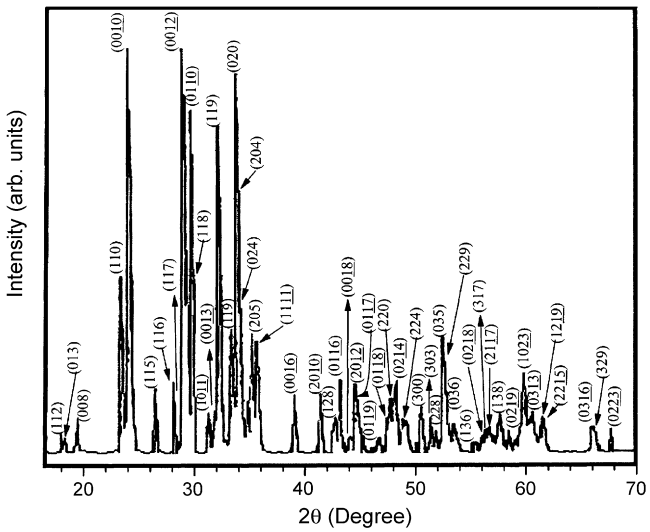

Fig. 5. Indexed X-ray diffraction pattern of the sample after the final sintering at room temperature.

3.4. Thermal properties measurements

After the preliminary characterization of the samples and existence of almost a single phase, large disc-shaped samples (28 mm diameter and 11 mm thickness) were used for the thermal measurements. Fig. 6 shows the temperature dependence of the thermal conductivity λ. As the temperature decreases, the conductivity gradually decreases down to near T_c then remarkably increases below T_c. Further decrease in temperature was not possible, due to limitation of the cryostat used, to take the maximum in λ. This temperature dependence agrees with the widely observed behavior of λ for the oxide superconductors [30–34].

Comparing the results between different laboratories, one notes that the thermal conductivity depends on a particular sample preparation process. The temperature dependence of the conductivity is really similar for all the samples [35,36]. So the order of magnitude of thermal conductivity (measured by non-steady state method in our case) is comparable to the results obtained by different authors (measured by steady-state methods).

Fig. 6 also shows the variation of measured thermal diffusivity κ with temperature for the sample. Between 294 K and T_c, κ increases very gradually with decreasing temperature. The increase of κ becomes very large around T_c and become very steep.

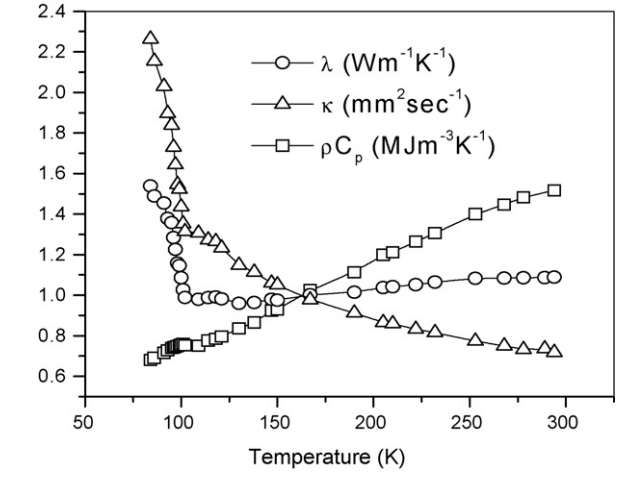

Fig. 6. Variation in thermal transport properties with temperature for the sample $Bi_{1.6}Pb_{0.4}Sr_{1.6}Ba_{0.4}Ca_2Cu_3O_y$.

The heat capacity per unit volume, ρC_p, calculated from the thermal conductivity measurements and thermal diffusivity measurements by using Eq. (1) is shown in Fig. 6. ρC_p decreases with decrease in temperature and near T_c a sizeable kink is observed. This jump is mostly due to the improved sharpness of the transition related to the reduction of intergrowth structure by adding Pb [37] and is improved by adding Ba in our case. Since the calculated lattice constants of our sample are similar to Bi-2223 composition so it is assumed that oxygen is 10, and then the composition becomes $Bi_{1.6}Pb_{0.4}Sr_{1.6}Ba_{0.4}Ca_2Cu_3O_{10}$. Also there is no change in the density of the superconducting sample in the studied temperature range so the value of specific heat C_p is calculated. The absolute value of C_p is 320 J mol^{-1} K^{-1} at 180 K and that is similar to already reported value of a similar composition [37,38]. Because the phonon contribution is by far dominant than the electronic contribution in the temperature range studied, the specific heat data were fitted by the following Debye formula:

$$C_{p\text{-ph}} = 9nR\frac{T^3}{\Theta_D^3}\int_0^{\Theta_D/T}\frac{x^4e^x}{(e^x-1)^2}\,dx, \tag{3}$$

where $C_{p\text{-ph}}$ is molar specific heat, x the reduced phonon frequency, n (=19) the number of atoms composing Bi(Ba) 2223 molecules, R the gas constant and Θ_D is the Debye temperature. Although a single Θ_D fitting fails to give a unified strict fitting over the entire temperature range, but $\Theta_D = 510$ K gives a satisfactory fitting between $T = 120$ and 230 K as is shown in Fig. 7.

3.5. Thermoelectric power

To check the calibration of this new apparatus (Fig. 2), thermoelectric power of copper was measured in the temperature range 85–310 K. Results of our measurements are shown in Fig. 8 indicating an agreement with the already published data [39]. The standard deviation in the data was between 0.01 and 0.22 μV K^{-1} and the difference between measurements done in this work and the already published [39] data were within 5%.

The thermoelectric power of the high-T_c superconducting sample was measured in temperature range 85–300 K. The thermoelectric power (S) reached zero within experimental uncertainty in superconducting state. The thermoelectric power increased with decrease in temperature and after reaching T_c value, thermoelectric power decreased strongly to zero value (Fig. 9). At high temperatures the thermoelectric power is almost linear. Thus we can use the Mott expression to determine the Fermi level [39,40]:

$$S = S_0 - \frac{\pi^2 k_B^2}{3|e|E_F}T \tag{4}$$

where S_0 is a constant. From the slope (-0.03145 μV K^{-2}) estimated by a linear extrapolation we have found the Fermi level to be 0.78 eV.

Similar profile for the same kind of superconductors is reported [41–46].

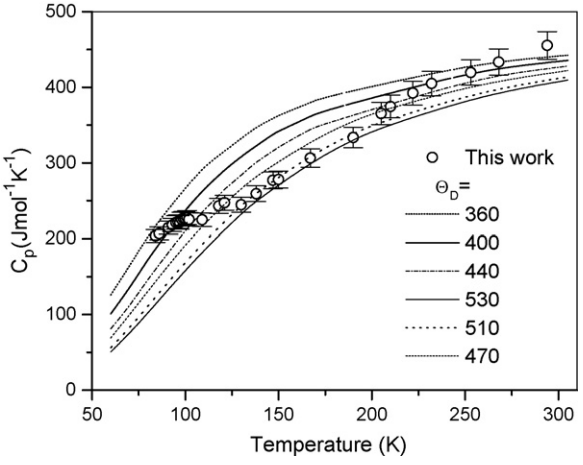

Fig. 7. The specific heat estimated from thermal conductivity (λ) and thermal diffusivity (κ). Calculated values for different values of Θ_D are also shown.

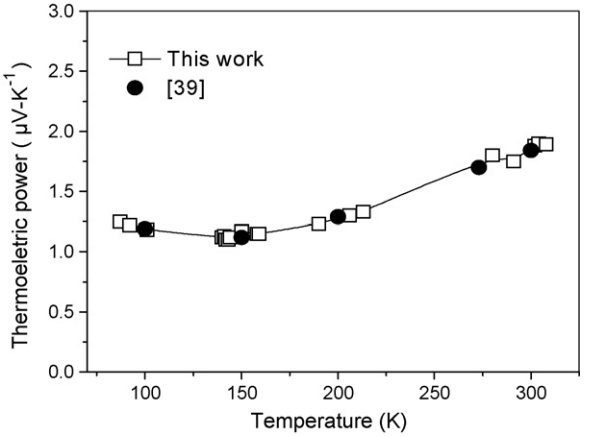

Fig. 8. Thermoelectric power of the copper sample with temperature.

3.6. Electrothermal conductivity

The electrothermal conductivity (P) is the thermoelectric power divided by the dc electrical resistivity and is given as

$$P = \frac{S}{\rho} \tag{5}$$

where S is the thermoelectric power and ρ is the dc electrical resistivity.

In the mixed state of a superconductor, the electrothermal conductivity is also defined as the measure of the electrical current density produced by a thermal gradient and is supposed to be independent of the magnetic field. We have utilized the former definition to calculate electrothermal conductivity and are shown in Fig. 9.

3.7. Figure of merit

Using the data of electrical resistivity, thermal conductivity and thermoelectric power, Figure of merit factor is calculated and is plotted in Fig. 10.

The Figure of merit is calculated from the expression [40]:

$$Z(T) = \frac{S^2(T)}{\lambda(T)\rho(T)} \tag{6}$$

where $Z(T)$ is the Figure of merit factor, $S(T)$ the thermoelectric power, $\lambda(T)$ the thermal conductivity and $\rho(T)$ is the electrical resistivity.

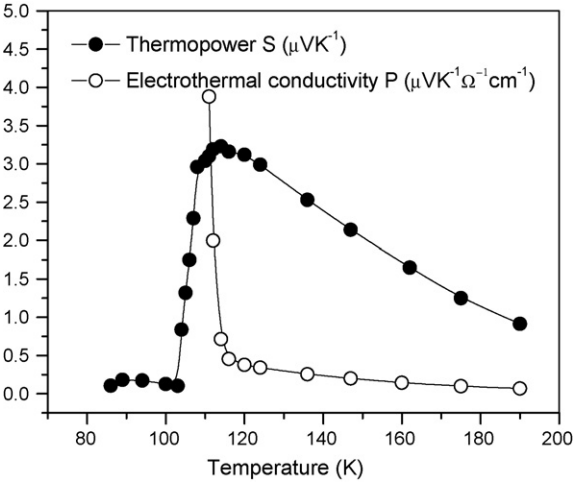

Fig. 9. Variation of thermoelectrical power (S) and electrothermal conductivity (P) with temperature for the sample.

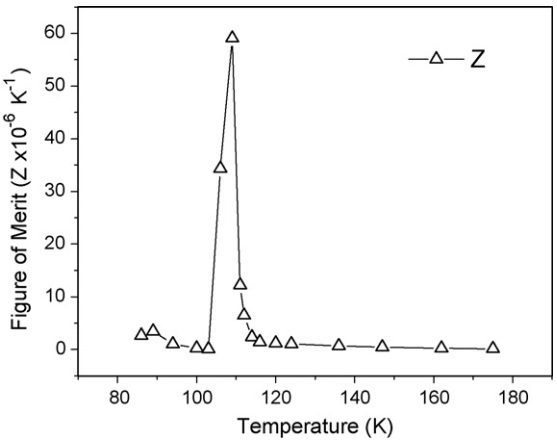

Fig. 10. Variation of Figure of merit factor (Z), with temperature.

Near critical temperature the Figure of merit present a remarkable peak for the samples. This peak is due to a quick drop in the electrical resistivity which occurs about 3 K before the drop in thermoelectric power. Outside the critical temperature region one can see that the curves of the Figure of merit and thermoelectric power are characterized by a similar behaviour near T_c. Similar trend of the Figure of merit is observed in the Bi-based high-T_c superconductors [40].

4. Summary and conclusions

The samples with nominal composition $Bi_{1.6}Pb_{0.4}Sr_{1.6}Ba_{0.4}Ca_2Cu_3O_y$ were prepared by a solid-state reaction method with controlled synthesis process to get the desired single phase. This composition was selected on the basis of experiments conducted by the authors with a similar composition [8]. The samples were almost a single phase with Bi-2223 high-T_c phase identified. All the three types of tests i.e. dc electrical resistivity, ac magnetic susceptibility and X-ray diffraction are in agreement with each other, all confirming almost a single Bi-2223 high-T_c phase. Single transition phase in the material and production of homogenous samples in large sizes favoured the advantageous transient plane source (ATPS) technique for thermal transport measurements. Thermal transport properties include thermal conductivity, thermal diffusivity and heat capacity per unit volume. Simultaneous measurement of thermal conductivity and thermal diffusivity makes it possible to estimate specific heat and the Debye temperature Θ_D. The simultaneous measurement also provides a useful check on the reliability and the consistency of the analyses. Thermal conductivity variation with temperature shows slight decrease initially and then a pronounced increase around T_c. A similar behaviour is observed in all hole-type CuO_2-plane superconductors and in all their structural forms. This effect is due to phonon [47] or quasiparticle scattering [48]. Thermal diffusivity shows a similar trend as that of the thermal conductivity. Heat capacity per unit volume decreases with decrease in temperature. Assuming density of the sample to be constant in the studied temperature range molar specific heat is also calculated. Specific heat jump around T_c is also very prominent. These results indicate a good crystalline structure and an optimal doping. Thermoelectric power was positive in this bismuth-based superconductor. The behavior of thermoelectric power of the sample was approximately linear with temperature as observed in other bismuth-based high-T_C superconductors. The superconducting transition started at 114 ± 1 K and after that, thermoelectric power decreased almost to zero value at 103 ± 1 K. The known value of the transition temperature of this sample measured from electrical resistivity was 110 ± 1 K. Therefore, the difference between thermoelectric transition temperature and resistivity transition temperature were almost in agreement within experimental errors. Electrothermal conductivity increases sharply near transition temperature. A maximum in the Figure of merit, of this ceramic superconductor, is around the superconducting transition temperature. It is then reduced to zero below critical temperature. This system can be useful for application in low-temperature Peltier devices in order to reach temperatures lower than the temperature of liquid nitrogen.

Acknowledgements

The author would like to acknowledge Higher Education Commission (HEC) Pakistan for the financial support for this research work. Dr. M. Maqsood and Prof. Dr. A. Maqsood are appreciated, for their useful suggestions.

References

[1] K. Remschnig, J.M. Tarascon, P.F. Miceli, G.W. Hull, Phys. Rev. B 43 (1991) 5481.
[2] V.P.S. Awana, S.K. Agarwal, B.V. Kumaraswany, B.P. Singh, A.V. Narlikar, Supercond. Sci. Technol. 5 (1992) 376.
[3] A. Maeda, T. Yabe, S. Takebayashi, M. Hase, K. Uchinokura, Phys. Rev. B 41 (1990) 4112.
[4] B. vom Hedt, W. Lisseck, K. Westerholt, H. Bach, Phys. Rev. B 49 (1994) 9898.
[5] A.V. Pop, R. Deltour, A. Harabor, D. Ciurchea, Gh. Ilonca, V. Pop, M. Todica, Supercond. Sci. Technol. 10 (1997) 943.
[6] N. Mori, J.A. Wilson, H. Ozaki, Phys. Rev. B 45 (1992) 10633.
[7] S.H. Kim, H.S. Kim, S.H. Lee, K.H. Kim, Solid State Commun. 83 (1992) 127.
[8] M.A. Rehman, A. Maqsood, Physica C 418 (2005) 121.
[9] B. Batlogg, High Temperature Superconductivity, Addison-Wesley, Redwood City, CA, 1990.
[10] S.E. Gustafsson, Rev. Sci. Instrum. 62 (1991) 797.
[11] A. Maqsood, N. Amin, M. Maqsood, G. Shabbir, A. Mahmood, S.E. Gustafsson, Int. J. Energy Res. 18 (1994) 777.
[12] M. Maqsood, M. Arshad, M. Zafarullah, A. Maqsood, J. Supercond. Sci. Technol. 9 (1996) 321.
[13] M.A. Rehman, A. Maqsood, J. Phys. D: Appl. Phys. 35 (2002) 2040.
[14] A. Maqsood, M.A. Rehman, V. Gumen, A. Haq, J. Phys. D: Appl. Phys. 33 (2000) 2057.
[15] M.A. Rehman, A. Maqsood, Int. J. Thermophys. 24 (2003) 867.
[16] M. Fee, Appl. Phys. Lett. 62 (1993) 1161.
[17] P.L. Richards, J. Appl. Phys. 76 (1994) 1.
[18] A.T. Leea, L.P. Richards, S.W. Nam, B. Cabrera, K.D. Irwin, Appl. Phys. Lett. 69 (1996) 12.
[19] Microsoft Encarta Encyclopedia, Microsoft Corporation, USA, 2003.
[20] P. Majewski, J. Mater. Res. 15 (2000) 4.
[21] U. Balachandran, A.N. Iyer, P. Haldar, J.G. Hoehn, L.R. Motowidlo, H. Maeda, Togano K (Eds.), Bi-based High-T_c Superconductors, Marcel Decker Inc., New York, 1996.
[22] M.A. Rehman, M. Maqsood, N. Ahmad, A. Maqsood, A. Haq, J. Mater. Sci. 33 (1998) 1789.
[23] D.X. Chen, J. Nogues, K.V. Rao, Cryogenics 29 (1989) 800.
[24] K.H. Muller, Physica C 159 (1989) 717.

[25] T. Ishida, R.B. Goldfarb, Phys. Rev. B 41 (1990) 8937.
[26] S. Celebi, Physica C 316 (1999) 251.
[27] G. Jasiolek, J. Gorecka, J. Majewski, S. Yuan, S. Jin, R. Liang, Supercond. Sci. Technol. 3 (1990) 194.
[28] B. Seeber, Handbook of Applied Superconductivity, vol. 1, Institute of Physics Publishing, Bristol/Philadelphia, 1998.
[29] B.D. Cullity, Elements of X-ray Diffraction, 3rd ed., Addison-Wesley Publishing Company, Inc., London, 1967.
[30] C. Uher, A.B. Kaiser, Phys. Rev. B 36 (1987) 5680.
[31] S.D. Peacor, C. Uher, Phys. Rev. B 39 (1989) 11559.
[32] K. Mori, M. Sasakawa, T. Igarashi, Y. Isikawa, K. Sato, K. Noto, Y. Muto, Physica C 162 (1989) 512.
[33] M.F. Crommie, A. Zettle, Phys. Rev. B 41 (1990) 10978.
[34] J.L. Cohn, S.A. Wolf, T.A. Vanderah, Phys. Rev. B 45 (1992) 511.
[35] D.M. Ginsberg, High Temperature Superconductivity, World Scientific Publishing Co. Pte. Ltd., 1992.
[36] M. Ikebe, H. Fujishiro, T. Naito, K. Noto, J. Phys. Soc. Jpn. 63 (1994) 3107.
[37] N. Okazaki, T. Hasegawa, K. Kishio, K. Kitazawa, A. Kishi, Y. Ikeda, M. Takano, K. Oda, H. Kitaguchi, J. Takada, Y. Miura, Phys. Rev. B 41 (1990) 4296.
[38] J.E. Gordon, S. Prigge, S.J. Collocott, R. Driver, Physica C 185–189 (1991) 1351.
[39] R.D. Barnard, Thermoelectricity in Metals and Alloys, Taylor & Francis Ltd, London, 1972.
[40] H. Bougrine, M. Ausloos, R. Cloots, M. Pekala, Proceedings of the 17th International Conference on Thermoelectrics IEEE, 1998.
[41] N. Mitra, J. Trefny, B. Yarar, G. Pine, Z.Z. Sheng, A.M. Hermann, Phys. Rev. B 38 (1988) 7064.
[42] G.H. Chen, G. Yang, Y.F. Yan, S.L. Jia, Y.M. Ni, D.N. Zheng, Q.S. Yang, Z.X. Zhou, Mod. Phys. Lett. B 3 (1989) 1045.
[43] C. Laurent, S.K. Patapi, S.M. Green, L. Luo, C. Politis, K. Durczewski, M. Ausloos, Mod. Phys. Lett. B 3 (1989) 241.
[44] A.J. Lopez, J. Maza, Y.P. Yadava, F. Vidal, F. Garcia-Alvarado, E. Morán, M.A. Senaris-Rodriguez, Supercond. Sci. Technol. 4 (1991) S292.
[45] S.M.M.R. Naqvi, S.D.H. Rizvi, S. Rizvi, S.M. Raza, Proceedings of the Fifth International Symposium on Advanced Materials, Islamabad, 1997.
[46] M. Pekala, A. Tampieri, G. Celotti, M. Houssa, M. Ausloos, Supercond. Sci. Technol. 9 (1996) 644.
[47] L. Tewordt, D. Fay, Th. Wolkhausen, Solid State Commun. 67 (1988) 301.
[48] M. Houssa, M. Ausloos, Physica C 235 (1994) 1483.